Self-Assembly of a Lamellar ABC Triblock Terpolymer Thin Film. Effect of Substrates

Kenji Fukunaga*

UBE Industries, Ltd., 8-1 Goi-minamikaigan, Ichihara, Chiba 290-0045, Japan

Takeji Hashimoto*

Department of Polymer Chemistry, Graduate School of Engineering, Kyoto University, Kyoto 606-01, Japan

Hubert Elbs and Georg Krausch

Lehrstuhl für Physikalische Chemie II, Universität Bayreth, D-95440 Bayreuth, Germany

Received July 12, 2002

ABSTRACT: We study the self-assembly in thin films of a lamella-forming polystyrene-*block*-poly(2-vinylpyridine)-*block*-poly(*tert*-butyl methacrylate) triblock terpolymer thin film on a polyimide substrate and compare it with the self-assembly of the same system on a native oxide silicon (SiO_x) substrate. In addition to scanning force microscopy, we performed cross-sectional transmission electron microscopy. Both polyimide and SiO_x substrates attract the polar P2VP middle block. However, significant differences between the two substrates were revealed: (i) the difference in the interaction strength between the substrate and the polymers caused a different configuration of P2VP chains adsorbed to the substrate and hence a different structure of the first layer, and (ii) the structure of the first layer influenced the self-assembly of the lamellae throughout the entire film. In contrast to SiO_x substrates, on polyimide substrates the lamellae with the equilibrium thickness were formed in one step through a new intermediate structure.

I. Introduction

Diblock copolymer melts order into novel morphologies with nanoperiodicity and various symmetries. This is attributed to *interplay* between short-range segmental interactions of their component block chains, common to corresponding polymer mixtures, and long-range interactions arising from "*block connectivity*" and resulting packing effects of the component block chains in the respective domains. This interplay is brought into much richer situations, thus creating much more rich variations in morphologies, for mixtures of two diblock copolymers with different compositions and/or molecular weights and ABC triblock terpolymers, for example.[1]

In the case of ABC triblock terpolymers, the short-range interactions compete each other among A, B, and C and so do the long-range interactions between A−B and B−C connectivities. These competing short- and long-range interactions further interplay to result in extremely rich varieties of morphologies.[2] In the case of unconfined thin films (with a free surface), there are extra competing short- and long-range interactions between air surface and the terpolymers and between substrate surface and the terpolymers, giving rise to even more rich interplays and competitions and hence parameters to control the morphologies. Here the long-range interactions may generally come into play on orientation of the microdomains in thin films, commensurability of domain spacing with the film thickness, etc.[3]

The substrate−segment interactions have been reported to significantly influence the microdomain ordering in diblock copolymer films.[4] Furthermore, thin films of the triblock terpolymer have recently been studied extensively.[5−8] In this paper and earlier one we focus on the effects of substrates on morphology of the unconfined thin films, by keeping a set of any other parameters such as polymers, film preparation conditions, ordering conditions, etc., unaltered. We aim to investigate whether equilibrium morphology (shape and orientation of domains) depends on substrates and how kinetic pathways to the equilibrium morphology are effected by substrates. For the studies we selected two substrates, native oxide covered silicon (SiO_x) and polyimides, widely used in electronics, and so forth.

We reported on the thin-film self-assembly of lamellar forming polystyrene-*block*-poly(2-vinylpyridine)-*block*-poly(*tert*-butyl methacrylate) triblock terpolymers (SVT) on SiO_x substrates.[9] Thin films were prepared by dip-coating. The as-prepared films exhibited a spongelike microphase-separated structure with a lack of long-range order, covered by a thin homogeneous layer of the lowest surface energy component on the free surface. Upon "annealing" the thin film in a common solvent vapor, the initial structure was transformed into a three-phase lamella structure oriented parallel to the plane of the film (parallel lamellae). The transformation between the two morphologies occurred via the following two-step process. The transformation into the parallel lamellae started to progress from the free surface of the film and, eventually, reached through the entire film (first-step ordering process). After prolonged treatment, the parallel lamellae were found to thicken to the thermodynamically stable thickness (second-step ordering process). The second-step ordering process was accompanied by macroscopic dewetting of the film from the substrate. In a region near the substrate, a thin, laterally microphase-separated layer was observed, which allowed the polar poly(2-vinylpyridine) (P2VP) middle block to adsorb at the polar SiO_x substrate. In

10.1021/ma021096f CCC: $25.00
Published on Web 03/28/2003

this case the adsorption of the P2VP block to the SiO_x surface is so strong that we were not able to remove the adsorbed copolymers by repeated washing with pure solvent. In the present study, we expand our investigations to another substrate in order to judge whether the kinetic pathway found for SiO_x is general for other substrates.

Polyimide is also widely used as a substrate in the field of electronics.[10] Polyimide has an excellent thermal and chemical stability as well as good mechanical flexibility. In contrast to the situation of the brittle and hard SiO_x/Si substrate, sample preparation for cross-sectional transmission electron microscopy (TEM) is quite straightforward for block copolymer films prepared on the flexible polyimide substrates. Furthermore, preliminary experiments had shown that polyimide selectively attracts the P2VP block similar to the situation observed on SiO_x.

In the present article, we report on the route of self-assembly of SVT thin films on polyimide substrates. The samples were investigated by cross-sectional TEM and by scanning force microscopy (SFM).[11] Although both substrates preferentially adsorb the middle block, remarkable differences are observed between polyimide and SiO_x substrates.

II. Experimental Section

II.1. Materials. The SVT triblock terpolymer was synthesized by sequential living anionic polymerization.[12] The molecular weight of the SVT used is 2.93×10^5, and the volume fractions are $\phi_{PS} = 0.18$, $\phi_{P2VP} = 0.39$, and $\phi_{PtBMA} = 0.43$ (see SVT1 in ref 9). Bulk samples obtained by a very slow drying of a THF solution exhibit a lamellar morphology.[13]

II.2. Film Preparation. Thin films of the SVT were deposited onto polyimide sheets (UPILEX-S, UBE Industries, Tokyo, Japan) by dip-coating from a 0.7 wt % solution in tetrahydrofuran (THF). The samples were pulled out at a velocity of about 10 mm/s. THF is a common solvent for the constituent homopolymers.[7] Since the polyimide substrate is soft, we were not able to measure the film thickness by scanning force microscopy (SFM) after purposely introducing a scratch into the film as applied on SiO_x substrates.[7,9] However, in some samples the film did not completely cover the polyimide sheet. Therefore, we were able to determine the film thickness of the copolymer relative to the bare polyimide surface by SFM to be around 200 nm. The film thickness determined from the cross-sectional TEM images of the sample did not significantly differ from the value determined by SFM.

Aiming to prepare significantly thinner films, we partially dissolved the 200 nm thick films described above by dropping a drop of pure THF and leaving it roll off the sample. The thickness of the remaining films ranged between 10 and 30 nm, and the films thus prepared will be referred to hereafter as ultrathin films. For preparation of ultrathin films on SiO_x, the SVT thin films prepared by dip-coating on SiO_x substrates were washed in pure THF. This procedure left a strongly adsorbed copolymer layer on the SiO_x substrate.[7,9] It should be noted that the same procedure could not be applied to the case of polyimide substrate, since the solvent removed the entire SVT thin film. Hence, we utilized the different method as described above to prepare the ultrathin film on polyimide. This difference may imply that the SiO_x substrate has much stronger attraction with the polymer than the polyimide substrate, as will be discussed in detail later. The ultrathin film on the SiO_x substrate did not change its structure from the as-prepared state by the solvent vapor treatment.

It should be noted that there was no change in the morphology of the as-prepared thin films upon annealing in a vacuum at elevated temperatures but below the temperatures where thermal degradation becomes significant, as detailed previously.[9] For equilibration the samples were therefore exposed to saturated THF vapor in a closed chamber kept at room temperature. The duration of the exposure was varied. During the solvent vapor treatment, the macroscopic shape of the film was monitored by optical microscopy. After solvent vapor exposure, the sample was removed to ambient atmosphere and promptly dried. This equilibration procedure used was the same as that used for the thin films on the SiO_x substrate.[9] Preliminary experiments showed that the final morphology of the thin films may depend on the solvent which is used in the vapor treatment. However, we limit ourselves to the case of the THF vapor treatment in this article.

II.3. Scanning Force Microscopy (SFM). The samples were investigated by TappingMode scanning force microscopy (SFM) (Nanoscope III, Digital Instruments, Santa Barbara, CA).[11] All SFM measurements were performed in atmosphere at room temperature. Silicon tips with a curvature of some 5−10 nm (Nanosensors, Germany) were used. The sample surface was scanned in the repulsive tip−sample regime. The set point was optimized within a range allowing both stable imaging and at the same time minimizing sample deformation during the scan. The ratio A/A_0 (A is the set point and A_0 is the free oscillation amplitude) was set in the range 0.87−0.94. The drive frequency was set such that it caused a 10−15% decrease in the oscillation amplitude, being lower than the resonance frequency which was determined for the tip positioned at some 5 μm above the sample surface. The integral and the proportional gains were being set in the ranges 0.3−0.6 and 1.1−1.4, respectively. All constituent components of the SVT triblock terpolymer are glassy at the room temperature. Therefore, no viscoelastic contrast is expected, and the no contrast in the SFM phase images is observed between the different microphases, so that we adopted only the SFM *height* images. The contrast of the height images reflects the surface topography of the sample.

II.4. Transmission Electron Microscopy (TEM). The samples were embedded in a light-curing acrylic agent (Luxtrak, Toagosei Co., Tokyo, Japan) together with the polyimide substrate, and the matrix agent was subsequently cured by UV irradiation. During this procedure, the sample was cooled in order to minimize swelling by the curing agent. The specimens were trimmed and sliced to 140 nm thickness parallel to the film normal by using an ultra-microtom (ULTRACUT-S, Leica). Finally, the cross-sectional pieces were stained by OsO_4 vapor. TEM images were taken on a JEM-200CX (JEOL, Japan) microscope. Under the staining conditions used in this study, S, V, and T domains are expected to appear bright, dark, and gray, respectively, in the bright field TEM images.[9] The contrast of the images under the TEM was confirmed by the element spectroscopic TEM with a JEOL-200FX equipped with a Gatan electron energy loss filter and imaging system (TEM-EELS) operated at 200 kV (though images not shown here). The Os mapping with TEM-EELS together with the bright field images of the three-phase lamellae unequivocally determined that the S phase (brighter phase) contains less Os than the T phase (darker phase), while the V phase contains the largest.

III. Results

III.1. Initial Structure in the As-Prepared Film. Figure 1 shows the time evolution of the microdomain structure of the SVT thin film as observed with cross-sectional TEM. In the right-hand part of Figure 1, the respective structures are schematically sketched for clarity. Figure 1a shows the TEM image of the as-prepared film. Dark domains appear to form a texture within a gray matrix. The texture has a characteristic spacing of about 70 nm. However, it does not show long-range order. The approximate position of the free surface is indicated by a broken line. The free surface of the thin film is covered by the component comprising the gray matrix. After staining in OsO_4 vapor, the T domains are expected to appear gray. Furthermore, the T block is the lowest surface free energy component in

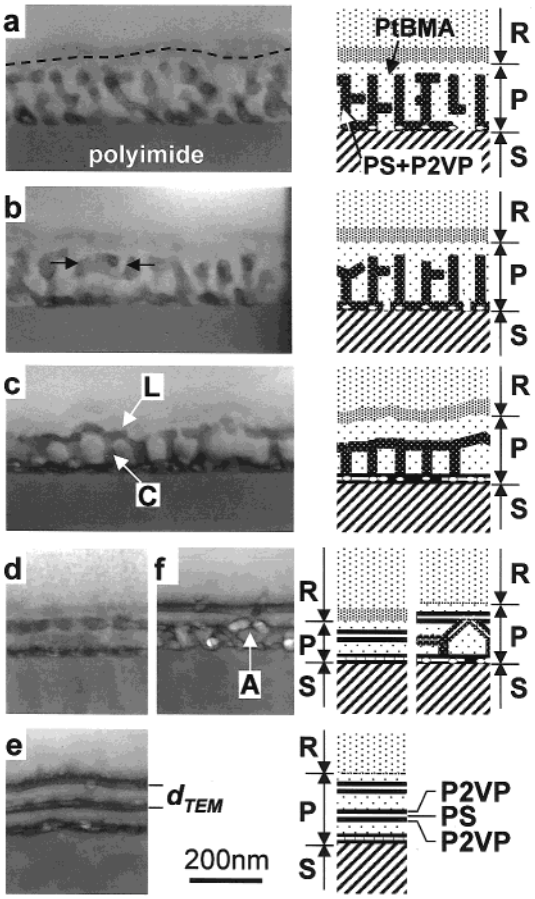

Figure 1. Cross-sectional TEM images showing the time evolution of the microdomain structure in a thin SVT film: as-prepared (a); after THF vapor treatment for 5 s (b), 10 s (c), and 1 min (d−f). The scale bar, common for all images, is shown in the bottom of the figure. PS, P2VP, and PtBMA appear bright, dark, and gray, respectively, in the TEM images. As a visual guide, the anticipated microdomain structures are schematically depicted on the right-hand side. The embedding resin, the substrate, and the SVT film are in the portion R, S, and P, respectively. In the schematic diagrams, the embedding resin, the substrate, PS, P2VP, and PtBMA are represented by dotted, slashed, white, black, and sparsely dotted areas, respectively. The embedding resin appears slightly darker near the interface to the SVT film which was indicated by black dashed line on the TEM image of part a. For the marker L, C, and A, see the text.

the SVT.[14] Hence, the gray matrix and the free surface are assumed to consist of T blocks. Finally, the substrate surface is in contact with both the gray matrix and the dark domains. Details of this microdomain structure will be discussed in section IV.1.

III.2. Solvent Vapor Treatment. III.2.1. Initial Stage. Figure 1b shows a cross-sectional TEM image of the SVT film subjected to THF vapor treatment for 5 s. The rather fragmented dark domains visible immediately after preparation (Figure 1a) tend to connect each other, leading to a more continuous structure. The arrows in Figure 1b indicate a portion in which the dark domains have increased continuity parallel to the film surface.

III.2.2. Intermediate Stage. On extended THF vapor treatment (10 s), the microdomain structure transformed further as shown in Figure 1c. Now the dark domain is found to completely cover the substrate surface, although in parts a and b the same portions were uncovered with the dark domains. Above this dark

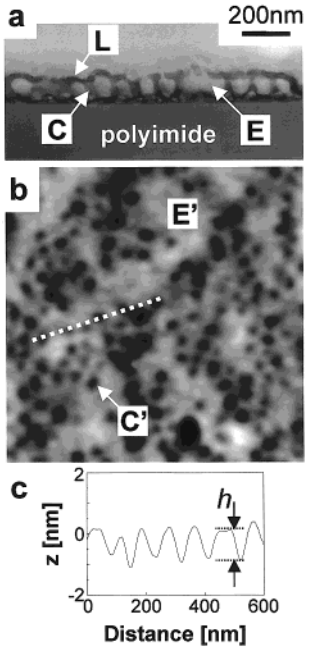

Figure 2. Intermediate structure shown in Figure 1c as observed by cross-sectional TEM (a) and SFM (b). The scale bar shown in (a) is common for both images. The height difference in (b) is in the range 0.0−3.0 nm. (c) represents the height profile taken along the dotted line in (b). For the markers, see the text.

layer adjacent to the substrate, a laterally continuous dark domain (indicated by L in Figure 1c) has developed from initially discontinuous domains. As we will show below, the continuous domain L can be considered to be a layer. In the thickness regime studied here, only two dark layers, i.e., the dark layer L and the dark layer on the substrate surface, were formed in this stage. The spacing of the two dark layers is 86 ± 16 nm. In addition to the layers formed parallel to the plane of the film, dark domains aligned perpendicular to the film plane are observed as well (indicated by C in Figure 1c). These domains (C) are connecting the two parallel layers. They exhibit an average lateral spacing of some 70 nm.

To explore fully the microdomain structure, we have taken SFM images of the free surface of the films at the different stages of solvent vapor treatment. Figure 2 shows the cross-sectional TEM image (a) and an SFM height image (b) after 10 s solvent vapor exposure. Part c shows a height profile of the surface. The TEM image from Figure 1c is reproduced in the same magnification as the SFM image for direct comparison. The SFM image (Figure 2b) exhibits isolated depressions appearing on the free surface of the film. From the height difference between the bottom of the depression and the surrounding area we determined the apparent depth *h* of the depressions. The depth of the depressions 1.2 ± 0.1 nm is considerably smaller than their lateral size. From a Fourier transform of this image, the average spacing between the depressions is determined to be some 70 nm, which is similar to the spacing between the perpendicularly aligned domains in the cross-sectional TEM image (C in Figure 2a). The surface dots (depressions) seem to associate with the respective perpendicular domains. This finding suggests that the perpendicular domains are cylinders. In the SFM height image, there are some featureless, flat areas (E′ in Figure 2b), where no depressions are observed. Corresponding to the flat areas on the free surface, the TEM

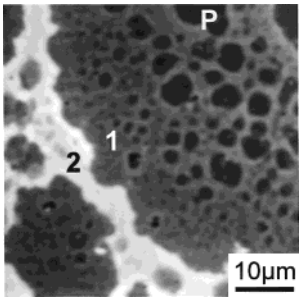

Figure 3. SFM height image of a thin SVT film after THF vapor treatment for 1 min. In some areas, the SVT dewets from the substrate and forms dry patches (P). The height difference is in the range 0−224 nm. The film shows a stepped surface comprising terraces of different height 1 and 2 (terrace 1 is lower).

image shows some regions (E in Figure 2a), where no perpendicular domains are observed over a distance considerably larger than their average spacing. The flat areas E′ are reflecting the in-plane structure of the dark domain L in Figure 2a. Hence, the domain L is considered to be a layer. The thin film shown in Figure 2 seems to form a meshlike structure (see Figure 3b in ref 15), where the dark cylinders (C) perforate the gray matrix, thereby bridging between the dark layer (L) and the dark layer on the substrate. The cylinders C seem to warp the layer L, thereby forming the slightly indented dots on the free surface. Why the cylinders may cause the dots on the surface will be discussed in more detail in section IV.2.

III.2.3. Final Stage. Figure 1d−f show cross-sectional TEM images of the thin film subjected to the THF vapor treatment for 1 min taken at three different spots. Eventually, the meshlike structure described in section III.2.2 transforms into a lamellar structure oriented parallel to the film surface. As shown by the difference between parts d and e of Figure 1, the thin film has developed areas with different stacking number of the lamellae. The spacing of the lamellae d_{TEM} is some 67 nm, which has become narrower than that of the two dark layers in Figure 1c. The perpendicular domains (C) seen in Figure 1c do no longer exist at this state. Figure 1f shows buckling of the lamella (A) found near the area shown in Figure 1e.

SFM height images (Figure 3), corresponding to the state shown in Figure 1d−f, taken over a larger lateral area indicate dewetting of the SVT thin film from the substrate. In some areas, dry patches appeared (indicated by P). Inside of the dry patches we find a surface roughness of some 0.2 nm, which is same as the bare polyimide surface. This flat area is quite dissimilar to the surface of SVT ultrathin films which will be described in the next section (III.3). Hence, the bare substrate seems to be exposed to air in the dry patch. Formation of the dry patches is indicative of a weak adsorption of the SVT to the polyimide surface.

An *autophobic* dewetting[16] of the thin film leads to a stepped surface indicative of a thickness quantization of the thin film.[17] Figure 3 shows areas 1 and 2 with well-defined thickness. The step height d_{SFM} between the areas 1 and 2 is 70 ± 4 nm, which coincides well with the spacing of the lamellae d_{TEM} in Figure 1e. The local structure near a step was observed by cross-sectional TEM (Figure 4). As a visual guide, the microdomain structure is schematically sketched in both the right- and left-hand parts of the figure. In the TEM

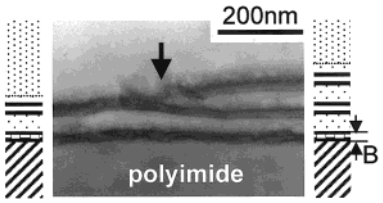

Figure 4. Cross-sectional TEM image of a thin SVT film showing a step (indicated by black arrow) that is accompanied by the dislocation core near the free surface. The lamellar structure is schematically shown on the both right- and left-hand side of the figure. The meaning of the schematic diagrams is same as in Figure 1. In the vicinity of the substrate, a laterally inhomogeneous layer (B) is observed.

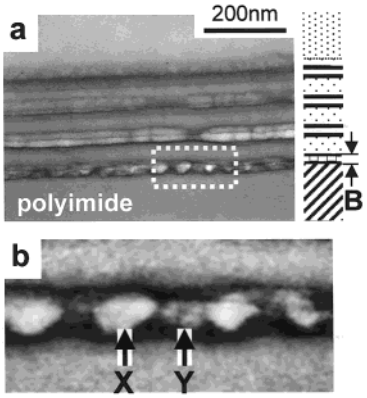

Figure 5. Cross-sectional TEM images of a thin SVT film after a THF vapor treatment for 1 day (a). As a visual guide, the anticipated structure is schematically shown on the right-hand side of (a). The meaning of the schematic diagrams is same as Figure 1. The meaning B is same as in Figure 4. (b) is a zoom-up of a portion indicated by the white dotted square in (a).

image, it is manifested that an edge-dislocation type defect has formed in the lamellar structure to enable quantization of the local film thickness. We note that the defect is located near the free surface of the film rather than near the substrate.

Figure 5a shows a cross-sectional TEM image of a sample subjected to the THF vapor treatment for 1 day. All three phases can clearly be distinguished in the TEM image. A schematic diagram of the lamellar structure is displayed on the right-hand part of the figure as a visual guide. Compared with Figure 1d−f, the ordering of the lamellae is somewhat improved after the extended treatment. However, the spacing of the lamellae does not change. We therefore conclude that on the polyimide substrate the equilibrium lamellae are formed in a one-step ordering process. This reveals a remarkable difference to the case of SiO_x substrates, where the lamellae formed initially thickened after an extended solvent vapor treatment (two-step ordering process).[9] This point will be discussed in detail in section IV.5.

In the vicinity of the polyimide substrate, the SVT forms a laterally inhomogeneous layer (B). The lateral inhomogeneity was already shown in Figure 1d−f as bright discrete domains in the dark domains on the substrate. Figure 5b shows a zoom-up of a part indicated by the white dotted square in Figure 5a. In the layer B, it seems that two kinds of bright domains with different brightness (indicated by X and Y in Figure 5b) are ordered in a row within the dark layer. This special structure seems to be induced by the substrate.

III.3. Ultrathin Films. Since the microphase structure of the SVT in the immediate vicinity of the

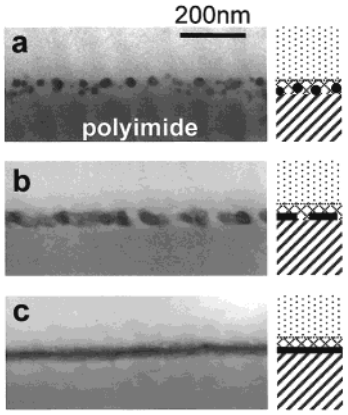

Figure 6. Cross-sectional TEM images showing the time-evolution of self-assembly in an ultrathin SVT film: as-prepared (a), after THF vapor treatment for 5 s (b), and 1 min (c). The scale bar, common for all images, is shown in the top of the figure. As a visual guide, the anticipated structures are schematically depicted on the right-hand side. In the schematic diagrams, the embedding resin, the substrate, the matrix comprising PS and PtBMA, and P2VP are represented by dotted area, slashed area, area of crosshatching, and black area, respectively.

substrate is a key to understanding layer B in Figure 5, we explored ultrathin films of SVT prepared by the method described in section II. The self-assembling process of the ultrathin film was observed by cross-sectional TEM as a function of the THF vapor treatment time (Figure 6). As a visual guide, the anticipated microdomain structures are schematically sketched in the right-hand part of Figure 6. Part a shows the cross-sectional TEM image of the as-prepared ultrathin film. P2VP (V) domains appear as isolated dark microdomains. PS (S) and PtBMA (T) microdomains are considered to establish the bright matrix but are not distinguished in the TEM image. Parts b and c of Figure 6 show cross-sectional TEM images of the ultrathin film subjected to THF vapor treatment for 5 s and 1 min, respectively. The isolated V domains seem to merge with increasing time of the THF vapor treatment. Eventually, the V domains form a continuous layer on the substrate surface, as shown in Figure 6c. A bright layer which may comprise S and T domains is seen on top of the V layer. However, S and T domains could not be identified.

Figure 7 shows the ultrathin film after THF vapor treatment for 1 day. In the figure, the cross-sectional TEM image (part a) and the SFM height image (part b), recorded with the same condition as in Figure 2b, are presented at the same magnification. The TEM image looks very similar to the one displayed in Figure 6c and shows a continuous V layer on the substrate and a bright layer on top. Within the bright layer, it is hard to distinguish between S or T microdomains, although some portions with different brightness are observed in the bright layer. On the other hand, the SFM height image (Figure 7b) shows stripelike corrugations on the free surface. The inset shows a Fourier transform of the SFM height image, and the characteristic wavelength of the corrugations is determined to be 77 ± 5 nm. Since the bright layer in Figure 7a comprises the free surface, the characteristic surface corrugations may indicate the microphase separation of S and T blocks comprising the bright layer. In the ultrathin film, it seems that (i) the V blocks are adsorbed to polyimide surface and forming a layer and (ii) S and T blocks are microphase-separated

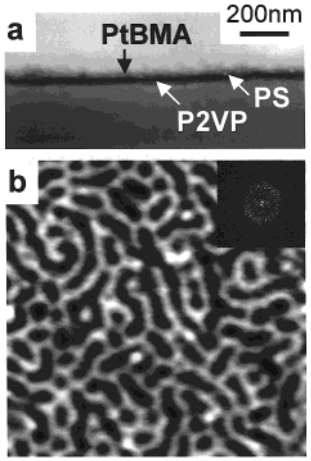

Figure 7. Ultrathin film structure as observed by cross-sectional TEM (a) and as observed by SFM (b). (b) shows an SFM height image recorded with the same way as in Figure 2b and the Fourier transform of the height image (inset). The scale bar shown in (a) is common for both images. The height difference in (b) is in the range 0.0−6.1 nm.

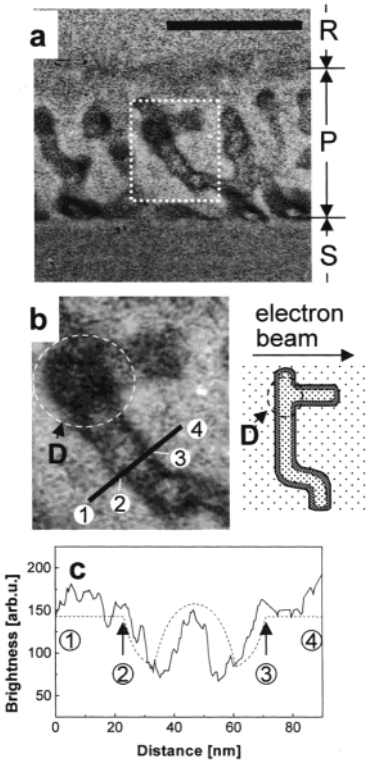

Figure 8. Cross-sectional TEM image of the as-prepared film (a). The meaning of R, P, and S is the same as in Figure 1. The scale bar in (a) represents 200 nm. The area indicated by the white dotted square in (a) is zoomed up in (b). (c) shows the TEM contrast (brightness) along the black line shown in (b). In (b) and (c), the positions indicated by markers 1−4 correspond to each other. The coaxial cylinder model is schematically depicted on the right-hand side of (b). See text.

with short range order on top of the V layer. This structure seems to correspond to the lower half of B layer shown in Figure 5.

IV. Discussion

IV.1. Structure of the As-Prepared Films. We start our discussion with the initial structure formed on the polyimide substrate. Figure 8a is an enlargement of Figure 1a, which shows the structure of the as-

prepared film. Branched dark domains appear in a gray matrix. Microphase separation seems to be completed locally; however, long-range order of the microdomains is not yet attained. Note that the SVT exhibits a lamellar equilibrium bulk structure. In the as-prepared film, nonequilibrium structures seem to be trapped kinetically. Figure 8b shows a zoom-up of a part of the branched dark domain indicated by the white dotted square in Figure 8a. Here, the dark domain appears to be darkest near the interfaces to the gray matrix. This feature is clearly revealed in Figure 8c, where the spatial distribution of the TEM contrast along the black line in Figure 8b is shown by the solid curve.

Now, we aim to model the microdomain structure leading to the characteristic contrast profile shown in Figure 8. If only the T blocks form the gray matrix, the dark domains have to be composed of the S and V blocks. Noting that S (V) domain appears bright (dark) in the TEM image, we may assume that S and V blocks are segregated to the core and the shell of the dark domain, respectively. This leads us to construct a core/shell cylinder model composed of an S core within a V shell. The model is schematically represented in the right-hand part of Figure 8b. Assuming this model for the microdomain structure of the cross-sectional piece for TEM, we calculated the intensity of the electron beam transmitted through the cross-sectional piece (Appendix). The calculated TEM contrast is shown by the dotted line in Figure 8c. The calculated contrast well reproduces the characteristic feature of the experimental contrast profile (solid line). In Figure 8b, a round area (surrounded by the dotted line with mark D) appears particularly dark. In terms of the core/shell cylinder model, the dark area D can be understood as the contrast caused by a cylinder portion with its axis oriented parallel to the electron beam (see the schematic diagram in the right-hand part of Figure 8b).

IV.2. Self-Assembly Induced by Solvent Vapor Treatment. On polyimide substrates, the SVT lamellae are formed in a one-step ordering process (section III.2). Figure 9 shows schematically the ordering process from part i to iv. In the as-prepared state (part i), the SVT forms the spongelike structure (see Figure 7 in ref 15). The structure is supposed to be composed of the coaxial cylinders with an S core and a V shell embedded within a T matrix (section IV.1). The cylinders are separated by a characteristic spacing λ of ~70 nm. The spacing λ resembles the lamella spacing d of the final state (Figure 9iv). It seems that the initial distorted structure has already programmed the characteristic spacing of the final structure.

In part ii, the cylinder network formed in the initial state transforms into an intermediate meshlike structure comprising the layer L (composed of V, S, and V three layers) and the core/shell cylinders (C) perpendicular to the layer L. This transformation may be driven by the change of mean curvature of the cylinders in such a way that the cylinders parallel to the film surface flatten or increase the planarity of their interfaces parallel to the film surface. This process increases the area fraction of the V and S phase and decreases the area fraction of the T phase in the thin L layer thus formed. As the transformation from the cylinders to the platelets proceeds, the meshlike structure is eventually formed. It seems that the some perpendicular cylinders (C) are left unchanged and form the perforating domains through the T matrix (M). During the THF vapor

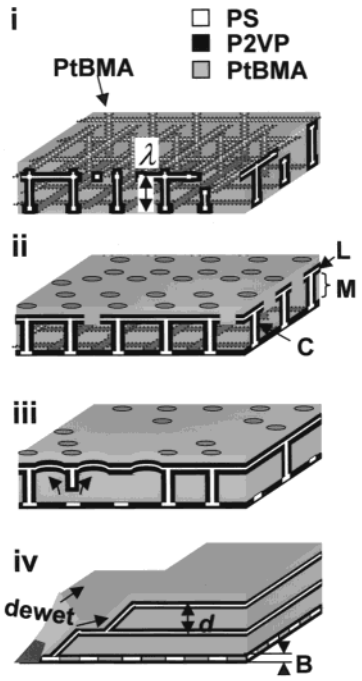

Figure 9. Schematic diagram of the lamellar formation process in the thin SVT films on polyimide substrates. In the initial stage (i), the triblock terpolymer forms a distorted interconnected core/shell cylinder structure. In the second stage (ii), the core/shell cylinder network is transformed into the intermediate meshlike structure comprising the layer (L) and the core/shell cylinders (C) perpendicular to the layer L. The cylinders C are perforating the T matrix layer (M). In the third stage (iii), the perpendicular cylinders C are transformed and incorporated into the layer L. In the fourth stage (iv), the thin film dewets from the substrate and some extra layer is formed on the free surface of the film, leaving bare substrate surface area shown by the dark area in the left edge of (iv).

treatment, S and V domains constituting the cylinders take up more THF than the T domain due to the solvent selectivity.[6] After the solvent removal, therefore, the cylinders are considered to shrink more than matrix M. Consequently, the depressions as observed in Figure 2b are expected to develop on top of the cylinders (C). Different surface tensions between the block components may also play a role for this, although the precise mechanism is not known yet. It should be noted that such a meshlike structure has never been observed on a SiO_x substrate.[9]

As shown in the change from part ii to part iii, the perpendicular cylinders C are transformed and incorporated into the layer L. Here, the cylinders C seem to act as channels for mass transport within the T matrix phase M, thereby transporting S and V blocks to the layer L. Hence, the meshlike structure may be essential for the observed one-step lamella formation. The transformation of the cylinders C into the layer L increases the interface area of the layer L. However, the surface area of the sample, i.e., the area of the layer L, cannot become larger during this transformation. This limitation induces an in-plane pressure to the layer L and may cause the buckling of the layer as observed in Figure 1f (indicated by A). This process costs a free energy penalty. Therefore, the system will further transform to minimize the free energy.

Finally, some extra lamella is formed on the free surface (see the change part iii to part iv). The defect associated with the extra layer is formed on the free surface rather than near the substrate. The cylinders

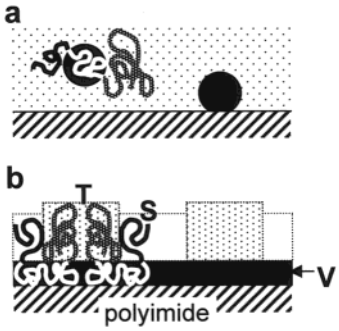

Figure 10. Schematic diagram showing the conformation of the SVT chain in the ultrathin film: as-prepared (a); after THF vapor treatment for 1 day (b). The dotted area in (a) represents the matrix comprising PS and PtBMA.

no longer exist, and the lamellar structure with the spacing *d* is formed throughout the entire film. At the same time, a multilayered film is formed as a consequence of dewetting of the SVT from the polyimide surface. The portion in the vicinity of the polyimide substrate has formed a laterally inhomogeneous layer B shown in Figure 5. The layer B will be discussed in section IV.4.

IV.3. Structure at the Boundary to the Substrate: Ultrathin Films. In this section, the structure of ultrathin film on polyimide substrates is discussed in comparison to what was found on SiO_x substrates. This comparison is essential for a discussion of the effects of the different substrates on the self-assembly process.

As seen in Figure 6a, the ultrathin film in the as-prepared state seems to form isolated V microdomains in a matrix of the other two blocks as schematically shown in Figure 10a. On THF vapor treatment, the V blocks first form a layer completely covering the polyimide surface (Figure 6c), indicating that the V chains are selectively attracted by the polyimide. Subsequently, as seen in Figure 7, S and T blocks microphase-separate on top of the V layer. Figure 10b schematically shows the chain conformation of the SVT. The ultrathin film is supposed to be a monomolecular film.[18]

Figure 11 shows the structure of the monomolecular SVT film on the polyimide (a-1) and on the SiO_x substrate (b-1). On the polyimide substrate (Figure 11a-1), S and T blocks form periodic phase-separated domains across their common interfaces on top of V layer as schematically shown in part a-3. The height profile measured along the white line on the SFM height image (part a-1) is shown in part a-2. Here, the vertical axis represents the height from the substrate surface. The height profile in part a-2 shows areas of two different height levels (A and B). As mentioned in section IV.2, after the THF vapor treatment, S domains are considered to shrink more than T domains due to the solvent selectivity.[6] Furthermore, the T block has a larger radius of gyration than the S block. Hence, in the monomolecular film, the T block is expected to be more protruded than S block on top of the V layer. The higher (A) and lower area (B) are therefore assumed to correspond to T and S microdomains, respectively. Part a-3 displays schematically the chain configuration of the SVT on the polyimide substrate in order to highlight a comparison with that on the SiO_x substrate (part b-3) to be discussed below.

On the SiO_x substrate, isolated microdomains are observed in the SFM height image (part b-1). Here, the

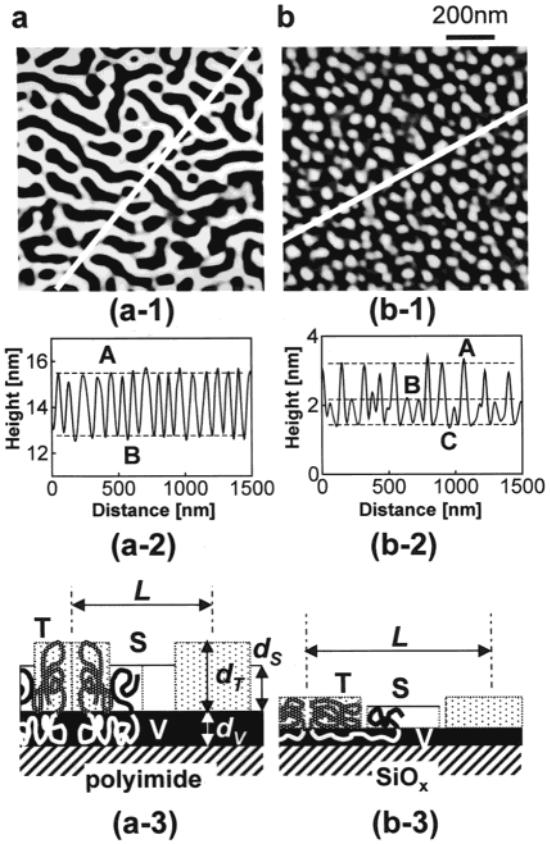

Figure 11. SFM height image of a monomolecular SVT film on a polyimide substrate (a-1) and on a SiO_x substrate (b-1) recorded in the same way as in Figures 2b and 7b. The height difference in (a-1) and that in (b-1) are in the ranges 0.0−6.1 and 0.0−3.6 nm, respectively. (a-2) and (b-2) show height profiles along the white lines in (a-1) and (b-1), respectively. (a-3) and (b-3) show schematically the chain configurations of the SVT on the polyimide substrate and on the SiO_x substrate, respectively. A part of the SFM height image in Figure 7b is zoomed up and reproduced in (a-1) for direct comparison.

surface profile seems to show areas of three different height levels (A, B, and C). As in the case of polyimide substrate, V blocks form the first layer on the SiO_x substrate due to the selective adsorption. On top of the V layer, S and T blocks are forming microdomains, which do not seem to have common interfaces. Hence, the height of the lowest level (C) in part b-2 is expected to correspond to the top of the bare V layer. Noting that the gyration radius of the T block is larger than that of the S block, it is expected that the more protruded area A and the less protruded area B correspond to T and S microdomains, respectively. From the SFM height image in part b-1, the volume of regions A and B is roughly estimated to be 710 and 180 nm^3, respectively. The volume of a single block chain of T and S is 210 and 79 nm^3, respectively. Therefore, two to four block copolymer chains may be forming the respective protrusions. The expected chain configuration is schematically depicted in part b-3. The bare V layer corresponding to the region C in part b-2 may be observed due to the expanded chain conformation of V blocks in the two-dimensional space on the substrate which increases the end-to-end distance of V blocks, as will be detailed below.

From the cross-sectional TEM image (Figure 7a), the thickness of V layer (d_V) is estimated to be around 6 nm for the case of the polyimide substrates. This value is considerably larger than the one observed on SiO_x

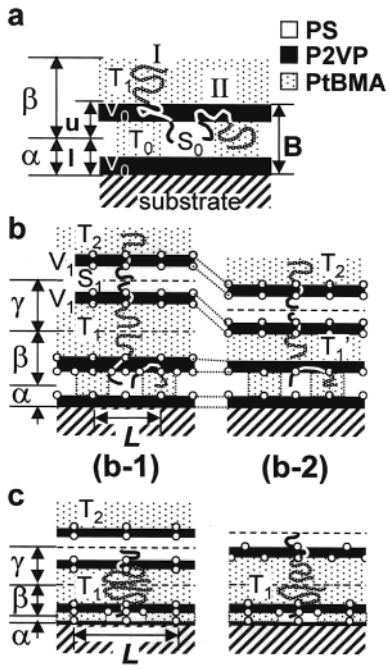

Figure 12. Model of the chain configurations of the SVT in a thin film on polyimide substrate (a, b) and on SiO_x substrate (c). I and II indicate two types of the chain configuration in the second molecular layer. The circles shown on the interfaces of the V layers ($V_0 + V_1$) represent the junction points between S and V and between V and T. α, *β*, and *γ* designate the first, second, and third molecular layers from the substrate surface. u and l designate upper and lower half of layer B. See text.

substrates (the height of the level C in Figure 11b-2 being only 1.3 nm). This finding indicates that on the polyimide the V block is less collapsed toward the substrate and less expanded parallel to the substrate compared to the situation on SiO_x. That is, the substrates have a different interaction strength to the V segments. The middle block V is supposed to be less strongly adsorbed on polyimide surfaces than on SiO_x surfaces. The lateral spacing L of the condensed domains comprising S and T end blocks is smaller on polyimide substrates than on SiO_x substrates. It means that the area density of junction points on top of the V layer is higher on polyimide than on SiO_x. Therefore, S and T domains are expected to be more extended in the direction normal to the V layer on polyimide than on SiO_x. The heights of the T and S domains (d_T, d_S) on polyimide are found to be around 10 and 6 nm, respectively. On SiO_x, the values d_T and d_S are read from the surface height profile in Figure 11b-2 to ∼2.5 and ∼1 nm, respectively.

IV.4. Structure at the Boundary to the Substrate: Thin Film. In section IV.3, we discussed the SVT structure formed in the monomolecular film on polyimide and SiO_x substrate. The structure of the first layer on the substrate may have a laterally inhomogeneous composition profile, as indicated by layer B in Figure 9. The difference of a substrate has been considered to cause a difference in number density of the junction points between S and V and between V and T on top of the V layer. Let us extend the consideration to the lamellar layers formed on top of the layer B in Figure 9iv.

Figure 12a schematically shows the layer B that is composed of two V layers (V_0) and S and T domains (S_0 and T_0) in between the two layers V_0. Layer B is composed of the first molecular layer of the SVT adsorbed on the substrate and the second molecular layer of the SVT. The SVT chains in the first molecular layer are expected to take a configuration similar to the one discussed in the ultrathin films (section IV.3). By considering whether the junction points between V and T exist on the interface between the layer V_0 and the T lamella (T_1), the configurations of the SVT chains in the second molecular layer are classified into two types: (i) configuration I: S block is confined in the S domain (S_0) in the layer B, whereas T block is confined in the T lamella (T_1) on top of the layer B; (ii) configuration II: S and T block are both confined in the S_0 and T_0 domains, respectively, within the layer B.

In both configurations, the V block is confined in the layer V_0, which must be a monolayer of V blocks (when V block do not mix with S and T blocks).

Figure 12b shows two models (b-1 and b-2) of the chain configurations of the SVT in a thin film on a polyimide substrate. The upper half of the layer B (indicated by u in part a) in the model 1 shown in part b-1 comprises both the chains of configuration I and the chains of configuration II. Hence, some junction points between V and T exist on the interface between the layer B and the lamella T_1. The lamella T_1 is composed of two T blocks, which belong to the second and the third molecular layer. On the other hand, the upper half of the layer B in the model 2 shown in part b-2 comprises only the chains of configuration II. In this case, the junction point between V and T does not exist on the interface between the layer B and the lamella T_1'. Accordingly, the lamella T_1' is a single layer of T block chains in the third molecular layer. In this case, the lamella T_1' should be thinner than a T lamella (T_2) composed of the two T blocks. However, the experimental observations (Figures 1e and 5a) show that the thickness of the first T lamella is not so much different from that of the second or higher T lamellae. Hence, model 2 is hardly supported by the experiment, while model 1 seems more reasonable.

Now, we turn to the case of the SiO_x substrate. On the SiO_x substrate too, the observed thickness of the first T lamella is almost the same as that of the second T lamella. Hence, the chain configuration on SiO_x substrate is considered to be represented by the model 1 (Figure 12b-1). The model for the SiO_x substrate is schematically depicted in Figure 12c. The area density of junction points on the interfaces of the layers V_0 is expected to be significantly lower than that in the polyimide case. The low area density of junction points on the layer V_0 is inherited on the interfaces stacked over the layer V_0, unless two T blocks in T_1 lamella take an asymmetrical configuration as schematically shown in right-hand part of Figure 12c (lower T blocks being more compressed than upper T blocks). If we can exclude such a configuration of the chains, the lamellae on SiO_x substrates are considered to be thinner relative to those on polyimide substrate.

IV.5. Comparison of the Self-Assembly into the Lamellar Morphology on the Different Substrates. On both the polyimide and the SiO_x substrates, the spongelike structure formed in the as-prepared state is eventually transformed into a three-phase lamellar structure in the first step of the ordering process as shown in parts a and b of Figure 13, respectively. Both cases show surface-induced ordering and alignment of the lamellae. However, the thickness of the lamellae

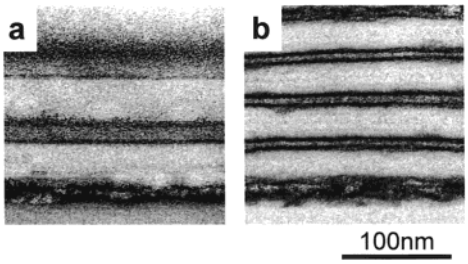

Figure 13. TEM images of SVT lamellae formed after THF vapor treatment for 1 min on polyimide (a) and on SiO_x (b).

formed in this step differs significantly on both substrates due to the different strength of the interactions between V blocks and the substrate.

On the SiO_x substrate, because of extensive adsorption of V segments onto the polar substrate surface, the density of the junction points between S and V and between V and T in the first layer is low as discussed in section IV.3. On the other hand, on the polyimide substrate, the density of the junction points in the first layer is rather high due to the weaker interactions between the V blocks and the substrate surface. In the first step of the ordering process, lamellae of equilibrium thickness are formed on the polyimide substrate. However, on the SiO_x substrate, thin lamellae are formed over several layers. Therefore, the substrate−polymer interactions exert a long-range effect, influencing the lamellar spacing across the entire thin film. This trend was found to be applicable to thin films with thickness in the range from some 100 nm to some 1000 nm in the case of the SiO_x substrate.[7,9]

The substrate may also influence the transformation pathway toward the lamellae. On the SiO_x substrate, the edge-dislocation-type defects were mostly observed near the substrate surface (see D in Figure 1d in ref 9). On the polyimide substrate, however, the defects were observed near the free surface (see Figure 4). The observed difference in the spatial distribution of the defects seems to reflect the different history for the lamella formation on both substrates.

On both substrates, the lamellar formed in the first-step ordering process shows dewetting from the substrate. However, the dewetting mechanism is different on both substrates. On the polyimide substrate, the dewetting was observed after the formation of equilibrium lamellae. The dewetting increases the film thickness by the formation of an extra layer on the free surface (Figure 9iv). On the other hand, on the SiO_x substrate, the dewetting of the thin film was observed at the same time when thickening of the thin lamellae occurred. The dewetting and the thickening of the lamellae increased the film thickness.

V. Conclusion

We studied the microdomain formation in SVT triblock terpolymer thin films on polyimide and SiO_x substrates. Both substrates preferentially attract the polar middle block (V). However, the V block is more strongly adsorbed by SiO_x surface than on the polyimide surface. This difference in the interactions between the V blocks and the substrates is found to result in different conformations of the middle V block adsorbed to the substrate and to cause different configurations of the SVT chains in the first layer adjacent to the substrate. The experimental observations revealed that the microphases in the first layer significantly depends on the substrate. This difference in the first layer influences several layers stacked on top of the first layer and to influence the pathway toward the equilibrium.

On SiO_x substrates the V blocks in the first layer are strongly adsorbed and hence take an expanded conformation parallel to the surface but compressed normal to the surface. As a consequence, thin lamellae are formed throughout the entire film during the first-step ordering process. The compressed lamellae thicken in the extended vapor treatment, which is accompanied by dewetting, showing a second step of the ordering process into lamellae with the equilibrium thickness. The dewetting, however, leaves the ultrathin monomolecular layer on the substrates.

On polyimide substrates, on the other hand, V blocks adsorb relatively weakly and hence do not take significantly distorted conformations. Therefore, the number density of junction points on top of the first V layer is larger than that on the SiO_x substrate. The large number density of junction points may be inherited over several interfaces on top of the first V layer, giving rise to a tendency toward formation of the lamellae more close to equilibrium lamellae in the first-step ordering process. The mobility of the V blocks on polyimide surface is higher than that on SiO_x surface, which facilitates a faster equilibration of the junction density on the substrate and interfaces and hence of the lamellar thickness. The equilibrium lamellae were formed by the one-step ordering process via formation of the meshlike structure as an intermediate structure. In this case too, dewetting occurs to result in thickening of the films, but it does not leave the ultrathin monomolecular layer. On both substrates, the three-phase coexisting lamellae are eventually formed parallel to the film surface. The first layer on the top substrate surface has a unique laterally inhomogeneous structure in both cases.

The discovery concerning the effects of substrates on kinetic pathways and time scale to achieve the equilibrium morphology may be quite important, since in many cases systems cannot attain equilibrium. The systems rather tend to be trapped in metastable states, and hence one must find methods to control nonequilibrium structures assisted by some basic principles of nonequilibrium phenomena to be further developed in future. We hope the present work will contribute to some extent along this line.

Acknowledgment. This work was financially supported by the Deutsche Forschungsgemeinschaft (SFB 481) and a Grant-in-Aid for Scientific Research (under Grant No. 12305060(A)) from Japan Society for the Promotion of Science. We are grateful to R. Stadler, V. Abetz, and E. Giebeler for supply of the block copolymers. We thank to K. Itoh for technical help for TEM observations. We also thank K. Yamauchi for help for TEM-EELS experiments.

Appendix. Calculation of the TEM Contrast for the Core/Shell Cylinder Model

For the calculation of the TEM contrast for core/shell cylinders the following parameters were assumed: $r_S = 13$ nm is the radius of the cylinder core composed of S blocks, and $r_V = 10$ nm is the thickness of the cylinder shell composed of V blocks. Here, the r_S and r_V were estimated so as to satisfying the volume fractions in the triblock terpolymer $[r_S/(r_S + r_V)] = [\phi_S/(\phi_S + \phi_V)]^{1/2}$, and

$2(r_S + r_V) = w$, where w is the apparent width of the dark domain in Figure 8b (46 nm). The coaxial cylinder is embedded in the matrix composed of T blocks.

We define the extinction coefficient μ_{ext} for the electron beam, $dI/I = -\mu_{ext}\, dl$, where I is the intensity of the electron beam after passing through a distance l of the sample. To estimate the extinction coefficients for the constituent blocks, we used the cross-sectional image of the three-phase coexisting lamellae shown in Figure 5a. At each position of this image, the electron beam is considered to have passed the single component having the thickness ($l_0 = 140$ nm) of the TEM sample. Hence, from the brightness of S (V) lamellae $I_{0,S}$ ($I_{0,V}$), we determined the extinction coefficient in S (V) domain relative to that in the T domain.

$$\Delta\mu_{ext,i} = \mu_{ext,i} - \mu_{ext,T} = -\ln(I_{0,i}/I_{0,T})/l_0 \quad (i = S, V)$$

Using these values, we calculated the TEM contrast of the core/shell cylinder model as shown in Figure 8c by the dotted curve. Although the characteristic spacing of the domain (some 70 nm) is smaller than the thickness of the TEM sample, we assumed that the electron beam has crossed only one of the core/shell cylinders in the sample. This assumption that causes only a vertical shift of the calculated curve does not influence the characteristic feature of the curve.

References and Notes

(1) See for example: Hashimoto, T.; Yamaguchi, D.; François, C. *Macromol. Symp.*, in press (a special issue of IUPAC MACRO, Beijing, China, July 2002). Hashimoto, T.; Yamauchi, K.; Yamaguchi, D.; Hasegawa, H. *Macromol. Symp.*, in press (a special issue of IUPAC-PC2002, Kyoto, Japan, Dec 2002).

(2) Bates, F. S.; Fredrickson, G. H. *Physics Today* **1999**, *52*, 32. Zheng, W.; Wang, Z.-G. *Macromolecules* **1995**, *28*, 7215.

(3) Russell, T. P.; Coulon, G.; Deline, V. R.; Miller, D. C. *Macromolecules* **1989**, *22*, 4600. Coulon, G.; Deline, V. R.; Green, P. F.; Russell, T. P. *Macromolecules* **1989**, *22*, 2581.

(4) Huang, E.; Mansky, P.; Russell, T. P.; Harrison, C.; Chaikin, P. M.; Register, R. A.; Hawker, C. J.; Mays, J. *Macromolecules* **2000**, *33*, 80.

(5) Stocker, W.; Beckmann, J.; Stadler, R.; Rabe, J. P. *Macromolecules* **1996**, *29*, 7502. Böker, A.; Müller, A. H. E.; Krausch, G. *Macromolecules* **2001**, *34*, 6883. Rehse, N.; Knoll, A.; Konrad, M.; Magerle, R.; Krausch, G. *Phys. Rev. Lett.* **2001**, *87*, 35505.

(6) Elbs, H.; Fukunaga, K.; Stadler, R.; Sauer, G.; Magerle, R.; Krausch, K. *Macromolecules* **1999**, *32*, 1204.

(7) Fukunaga, K.; Elbs, H.; Magerle, R.; Krausch, G. *Macromolecules* **2000**, *33*, 947.

(8) Balsamo, V.; Collins, S.; Hamley, I. W. *Polymer* **2002**, *43*, 4207.

(9) Fukunaga, K.; Hashimoto, T.; Elbs, H.; Krausch, G. *Macromolecules* **2002**, *35*, 4406.

(10) Ghosh, M. K.; Mittal, K. L. *Polyimides: Fundamentals and Applications*; Marcel Dekker: New York, 1996.

(11) Zhong, Q.; Innis, D.; Kjoller, K.; Elings, V. B. *Surf. Sci. Lett.* **1993**, *290*, L688.

(12) Giebeler, E.; Stadler, R. *Macromol. Chem. Phys.* **1997**, *198*, 3815.

(13) Giebeler, E. Dissertation, Universität Mainz, 1997.

(14) The surface tension γ of PS and PtBMA is 40.7 and 30.4 mN/m, respectively (Wu, S. In *Polymer Handbook*, 4th ed.; Brandrup, J., Immergut, E. H., Grulke, E. A., Eds.; John Wiley & Sons: New York, 1999). For P2VP, $\gamma = 46$ mN/m is calculated by computational code Cerius^2-Synthia (Accelrys, San Diego, CA; see: Bicerano, J. *Predictions of the Properties of Polymers from their Structures*; Marcel Dekker: New York, 1993).

(15) Hashimoto, T.; Koizumi, S.; Hasegawa, H.; Izumitani, T.; Hyde, S. T. *Macromolecules* **1992**, *25*, 1433.

(16) Green, P. F.; Limary, R. *Adv. Colloid Interface Sci.* **2001**, *94*, 53.

(17) Liu, Y.; Rafailovich, M. H.; Sokolov, J.; Schwarz, S. A.; Bahal, S. *Macromolecules* **1996**, *29*, 899.

(18) Spatz, J. P.; Sheiko, S.; Moeller, M. *Adv. Mater.* **1996**, *8*, 513.

MA021096F